J. Fluid Mech. (2010), *vol.* 649, *pp.* 509–522.
doi:10.1017/S0022112009994101

Turbulent rotating convection at high Rayleigh and Taylor numbers

J. J. NIEMELA[1]†, S. BABUIN[1] AND K. R. SREENIVASAN[1,2]

[1]International Center for Theoretical Physics, Strada Costiera 11, 34014 Trieste, Italy

[2]Department of Physics and Courant Institute of Mathematical Sciences, New York University, NY 10012, USA

(Received 4 September 2009; revised 21 December 2009; accepted 21 December 2009)

We report heat transport measurements in a cylindrical convection apparatus rotating about the vertical axis. The aspect ratio was 1/2. The working fluid was cryogenic helium gas and the following parameter ranges applied: the Rayleigh number, Ra, varied in the range $10^{11} < Ra < 4.3 \times 10^{15}$, the Taylor number, Ta, varied in the range $10^{11} < Ta < 3 \times 10^{15}$, the convective Rossby number, Ro, varied in the range $0.4 < Ro < 1.6$ and the Prandtl number, Pr, varied in the range $0.7 < Pr < 5.9$. Boussinesq conditions applied quite closely. The heat transport for steady rotation, under all conditions of the present experiments, was smaller than that for the non-rotating case. When the rotation rate varied periodically in time, a sharp transition to a state of significantly enhanced heat transport was observed for modulation Taylor numbers $Ta^* \gtrsim 10^{14}$, where Ta^* is based on the peak value of the modulation angular velocity.

1. Introduction

The Rayleigh–Bénard convection is a paradigm for a number of natural and engineering flows in which a layer of fluid is heated from below and cooled from above. When this heating and cooling results in large enough unstable density gradients, a macroscopic flow is generated. This flow enhances heat transport far above the molecular limit. The vertical temperature difference, causing buoyancy force, is measured in terms of the Rayleigh number $Ra \equiv \alpha \Delta T g H^3/\nu\kappa$, where α is the isobaric thermal expansion coefficient of the fluid in the container, ΔT is the temperature difference between the bottom and top walls, g is the acceleration due to gravity and H is the vertical dimension of the convection cell. The kinematic viscosity and the thermal diffusivity of the fluid are denoted, respectively, by ν and κ. The ratio ν/κ is the fluid Prandtl number, Pr. The macroscopic flow becomes turbulent for large Ra. Rayleigh numbers as high as 10^{17} have been attained in laboratory experiments (Niemela *et al.* 2000) by using low temperature helium gas as the test fluid in a relatively large apparatus. For simple fluids operating under 'ideal' conditions, Ra and Pr determine the state of convection fully. However, other factors such as the geometry, aspect ratio and the thermal properties of the container materials can be expected to play some role in all laboratory experiments (see e.g. Ahlers, Grossmann & Lohse 2009). An advantage of cryogenic experiments, besides the favourable properties of the gaseous state of helium at these temperatures for

† Email address for correspondence: niemela@ictp.it

producing large values and ranges of Ra, is that artifacts due to the imperfect thermal boundary conditions are relatively small compared to experiments using common fluids such as water at room temperature. Specifically, the range of Ra in these experiments has been chosen to assure that even these small artifacts are minimal (see Niemela & Sreenivasan 2006 and references therein for this discussion).

One particular feature of large-scale geophysical and astrophysical flows is that convection is always accompanied by rotation, which introduces the Coriolis force. This is a major factor in such large-scale flows which are also strongly turbulent, e.g. oceanic and atmospheric flows, convection in the outer core and in the Sun and other stars. The relative strength of the dimensioned rotation Ω_D (in rad s^{-1}) is given by its non-dimensional form, $\Omega = (2\Omega_D H^2/\nu)$, which is a measure of the ratio of Coriolis force to viscous force and is the inverse of the Ekman number, Ek. It is customary to consider the Taylor number $Ta = \Omega^2$ also. A measure of the relative importance of Coriolis and buoyancy forces is given by the convective Rossby number $Ro = [Ra/(Pr\,Ta)]^{1/2}$, which can also be interpreted as the ratio of the rotation period to the buoyancy time scale. Rewriting Ro as $(2\Omega_D)^{-1}(g\alpha\Delta T/H)^{1/2}$ makes it clear that the only fluid property on which it depends is the expansion coefficient α in the combination $\alpha\Delta T$. The latter quantity varies over a range that is more or less similar for all experiments conforming to the Boussinesq approximation. Though it is not clear if exactly the same limits on $\alpha\Delta T$ apply to all fluids equally, it is reasonable to assume that they are of the same order. Thus, considering typical constraints on size and speed in academic laboratories, we can expect that the lower limit of Ro will be roughly of the same order of magnitude for them. What can be 'substantially' different are the Rayleigh and Taylor numbers themselves. One motivation for the present experiments is the possibility that the effect of rotation may depend on the state of convective turbulence (given by Ra and Pr), regardless of the relative values of the Coriolis and buoyancy forces (given by Ro). Indeed, this idea has been discussed in a recent paper by King *et al.* (2009) in which boundary layer ratios are shown to be more relevant in determining the effects of rotation on turbulent convection than the Rossby number itself. We will return to this point when we discuss time-varying rotation below.

The linear stability theory of rotating convection (e.g. Chandrasekhar 1961) says that the critical Rayleigh number increases with rotation. It is also known from the Taylor–Proudman theorem that convection in a rotating system away from the walls tends to arrange itself in vertical columns. Both these results suggest that rotation would inhibit heat transport. However, Rossby (1969) and a number of recent workers (Zhong, Ecke & Steinberg 1993; Julien *et al.* 1996; Liu & Ecke 1997; Kunnen, Clercx & Geurts 2006, 2008; Oresta, Stringano & Verzicco 2007; Stevens *et al.* 2009) have found that heat transport increases with rotation. This enhancement was attributed to the extra vertical circulation resulting from Ekman suction at the boundaries, although Kunnen *et al.* (2006) argued that large rotation rates would weaken and even reverse this tendency. These studies all correspond to moderate Rayleigh numbers by today's standards (below 10^9 in most). More recently, Zhong *et al.* (2009) demonstrated that the enhancement of heat transport diminishes with increasing Ra and decreasing Pr. Their experiments correspond to Ra between 10^8 and 1.8×10^{10}. As we shall see, the present results at higher Ra and Ta show that the enhancement effect under steady rotation not only vanishes but also reverses with increasing Ra and Ta, giving way to a slight suppression of heat transport even for moderate Pr.

The experiments to be reported here correspond to large Ra ($10^{11} < Ra < 4.3 \times 10^{15}$) and large Ta ($10^{11} < Ta < 3 \times 10^{15}$); the convective Rossby number varied between

0.4 and 1.6, so the Coriolis and buoyancy forces are comparable. For most of the range of Ra the Prandtl number remains constant at 0.7, as expected for a perfect gas, but increases to about 5.9 at the highest Ra used here. This increase occurs because the high end of the Ra regime has been attained by approaching the thermodynamic critical point of helium (see Niemela & Sreenivasan 2003*a*). For all conditions of steady rotation explored here, the heat transport is lower than that in the non-rotating case. An exception occurs under modulated rotation in which the fluid undergoes periodic spin-up and spin-down cycles of the rotation rate. It appears plausible that small-scale turbulence generated in the thermal boundary layer by strong deceleration in the spin-down part does not die away altogether during the acceleration of the following spin-up, thus decreasing the resistance of the thermal boundary layer to heat transport and enhancing mixing. This enhancement occurs for modulation Taylor numbers denoted by Ta^* – based on the peak modulation angular velocity – exceeding a transition value to be discussed below. The Rayleigh number appears to play a secondary role by setting the thickness of the thermal boundary layer: the enhancement in heat transfer also coincides with the estimated thermal boundary-layer thickness being of order of the rotationally induced Ekman layer thickness. Interestingly, this is a criterion adopted recently by King *et al.* (2009) to describe a transition between rotationally- and non-rotationally dominated convective dynamics.

Section 2 provides a brief description of the experimental apparatus. The main results are contained in § 3. Concluding remarks and future prospects are discussed in § 4.

2. The apparatus

Aside from the rotating platform, the apparatus is essentially the same as that described in earlier works (see e.g. Niemela *et al.* 2000). A thin-wall (0.267 cm) stainless steel cylinder of diameter 50 cm confines the fluid laterally while two 3.8 cm thick plates made of oxygen-free high-conductivity annealed copper, having a thermal conductivity of the order $1\,\mathrm{kW\,m^{-1}K^{-1}}$ at the measurement temperature, provide top and bottom thermal boundaries with a separation distance of 100 cm between them. The diameter to height aspect ratio, Γ, is thus $1/2$. A key feature of the apparatus is the ability to heat the plates uniformly, using distributed thin film heater elements. The controlled quantities are the heat flux at the bottom plate and the temperature of the top plate, connected to a cold high heat capacity reservoir filled with liquid helium. Here the connection to the top plate was made through an adjustable gaseous helium thermal link. The plate temperature was maintained constant by means of a resistance bridge and servo. To prevent stray heating by radiation, the convection cell was insulated by three outer thermal shields at various temperatures and residing in a common cryo-pumped vacuum space. The helium gas was nominally at 5 K and the wide range of Ra was achieved primarily by varying the pressure (or density) of the fluid.

Briefly, rotation was provided by placing the entire apparatus on a thick steel plate attached to a large slewing ring. Platform speed was measured and held constant by means of an optical encoder on the motor shaft and associated proportional–integral–derivative (PID) control. All measuring and data storage instruments are located on the rotating platform with the main power transferred via a heavy-duty rotating contact slip ring.

All measurements were initiated only after waiting for steady state conditions to develop. The waiting times varied with Ra, but were typically several hundred cycles

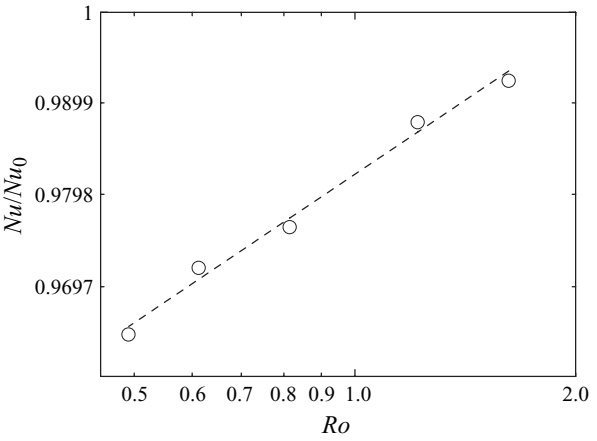

FIGURE 1. Log-log plot of Nu/Nu_0 versus Ro for $Ra = 4.3 \times 10^{15}$ and $Pr = 5.9$.

of the large-scale circulation, occasionally ranging up to a hundred thousand cycle times.

3. Results

3.1. *Heat transport under steady rotation*

The Nusselt number, Nu, is the ratio of the measured heat flux to that accomplished, for identical ΔT and H, by molecular conduction alone. For all conditions of Pr, Ro, Ra and Ta explored here, Nu is smaller than that without rotation, Nu_0. The Nusselt numbers reported here have been corrected for an adiabatic temperature gradient (see Tritton 1988), but not for finite sidewall and plate conductivity (Ahlers 2001; Verzicco 2002), for two reasons. First, one does not know the precise form of these corrections in the presence of rotation and, second, these corrections are exceedingly small for the non-rotating case in the present range of Ra (Niemela & Sreenivasan 2006). Subtraction of the parallel empty cell conduction up the sidewalls was made, however. The nominal procedure was to establish steady heating conditions and to measure Nu initially under non-rotating conditions; however, no history dependence was observed for either steady or time-varying rotation, within a measurement uncertainty of order 0.1 %. In the case of periodically modulated rotation, it was necessary to average measurements of Nu over integer numbers of modulation cycles after establishing statistically stationary conditions.

The change in the Nusselt number Nu from its value in the non-rotating case, Nu_0, is relatively small for moderate rotation corresponding to convective Rossby numbers close to unity. We illustrate this for the case of $Ra = 4.3 \times 10^{15}$ shown in figures 1 and 2, where Nu/Nu_0 is plotted against Ro and Ta, respectively, for the same moderate $Pr = 5.9$. For these data, relatively modest rotation rates up to 1.05 rad s^{-1} were used to avoid vibrations and large centrifugal forces; large magnitudes of Ta were obtained mainly by working under conditions of small kinematic viscosity, which could be altered over several orders of magnitude. (In experiments, the heating applied to the bottom plate is fixed, so the temperature difference ΔT will change slightly when the apparatus is set in rotation. Nu_0 corresponding to this new temperature difference is obtained by the interpolation of the local Nu–Ra relation for the non-rotating case.

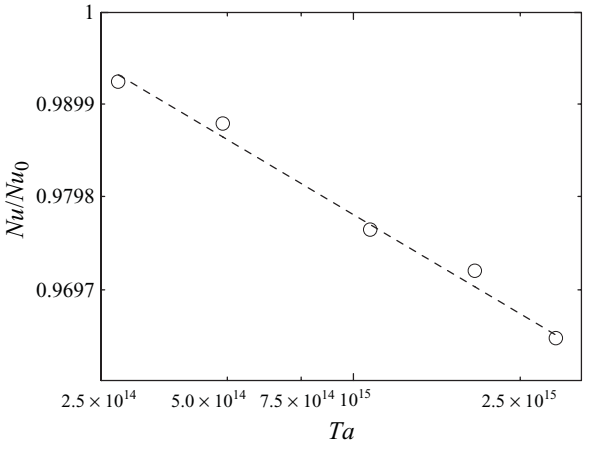

FIGURE 2. Log-log plot of Nu/Nu_0 versus Ta for $Ra = 4.3 \times 10^{15}$ and $Pr = 5.9$.

We note that present measurements for the non-rotating case agree well with past measurements of Niemela *et al.* 2000.)

The best fits to these rotation data,

$$Nu = 0.982 Nu_0 Ro^{0.024 \pm 0.001}, \tag{3.1}$$

$$Nu = 1.48 Nu_0 Ta^{-0.012 \pm 0.001}, \tag{3.2}$$

indicate a weak suppression of heat transport with increasing rotation. This suppression might initially appear to contradict results at moderate Ra, e.g. Liu & Ecke (1997) in water ($3 < Pr < 7$; $2 \times 10^5 < Ra < 5 \times 10^8$; $0.1 < Ro < 1.5$; $0 < Ta < 5 \times 10^9$), where an enhancement of heat transport was observed. The difference in the two cases cannot be attributed to differences in Prandtl number because it was matched in the present experiments to that of water (figures 1 and 2 correspond, in fact, to $Pr = 5.9$). These authors had already cautioned that their result – counter-intuitive in the light of Taylor–Proudman stabilization and the delayed onset of convection in the presence of rotation – was an example of the difficulty in applying intuition based on non-turbulent states to those at higher Ra. The present results, which are not entirely unexpected in view of the finding of Zhong *et al.* (2009) – conducted at higher Ra than that of Liu & Ecke (1997) – that the heat-transport enhancement diminishes at higher Ra, re-frame the general caution of Liu & Ecke (1997).

3.2. *Convection under conditions of periodically varying rotation rate*

The effects of periodic modulation of the rotation rate, resulting in continual cycles of spinning up and down, were investigated near the convective onset by Niemela, Smith & Donnelly (1991) and Thompson, Bajaj & Ahlers (2002). However, relatively little is known about such processes in strongly turbulent convective systems, where the diffusive boundary layers are many orders of magnitude smaller than the fluid-layer thickness and strong circulations and advected plumes exist, leading to a well-mixed interior (Niemela & Sreenivasan 2008). In this fully turbulent background, cyclic spin-up and spin-down conditions can have a significant effect on the heat transfer, as will be shown below. Here, we vary the rotation rate sinusoidally in time as

$$\Omega_D(t) = \Omega_D^* \cos(\omega t). \tag{3.3}$$

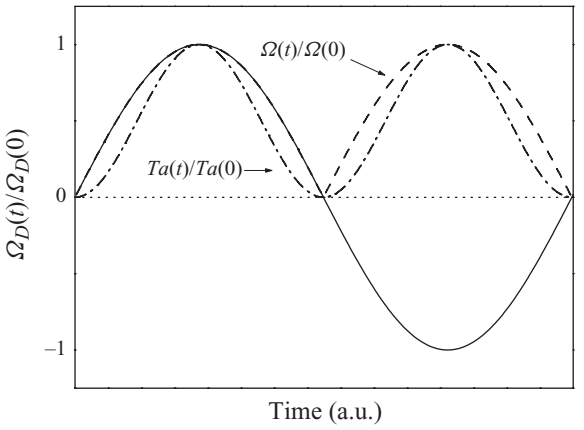

FIGURE 3. Schematic of the modulation, $\Omega_D(t)/\Omega_D(0)$ (solid line), $\Omega(t)/\Omega(0)$ (dashed line) and $Ta(t)/Ta(0)$ (dot-dashed line) versus time. Neither the Taylor number nor the dimensionless rotation rate Ω depends on the direction of rotation, so the modulation has an effective frequency of 2ω.

The rate at which the rotational speed is varied is set by ω, whose inverse was chosen to be on the order of the large-scale circulation time in the cell – this being one plausible time scale for turbulent convection. Very large or small ω would be characterized, respectively, by dominant Stokes layer development and associated viscous waves or quasi-steady conditions. The most important parameter for the present experiments is Ω_D^*, which is the peak rotation rate experienced by the flow during a cycle. Since the direction of rotation should not matter (if the effect of the Earth's rotation is assumed to be small), there should be an effective rectification, as observed in temperature signals which show the characteristic frequency 2ω (we shall discuss this later with reference to figure 8). We define the time-dependent dimensionless rotation rate $\Omega(t)$ (the inverse of a similarly time-dependent Ekman number) as

$$\Omega(t) = \frac{2\Omega_D^*|\cos(\omega t)|H^2}{\nu} \tag{3.4}$$

and the time-dependent Taylor number as

$$Ta(t) = \Omega(t)^2. \tag{3.5}$$

The parameters $\Omega_D(t)$, $\Omega(t)$ and $Ta(t)$ are plotted schematically in figure 3. The peak values of these quantities within a cycle will be used to characterize the modulated state, indicated by the superscript $*$:

$$Ta^* = \Omega^{*2} = \left[\frac{2\Omega_D^* H^2}{\nu}\right]^2. \tag{3.6}$$

Our goal was to measure the change in Nusselt number, ΔNu, defined by

$$\Delta Nu = Nu - Nu_0 \tag{3.7}$$

with varying Ω^* and Ra. As noted above, we averaged the measurements over integer number of modulation cycles after establishing statistically stationary conditions. Figure 4 plots the variation of ΔNu with Ω^*; for increasing Ω^*, we observe ΔNu to *decrease* slightly, up to a certain transition value, roughly $\Omega_c^* \sim 10^7$ (or $Ta_c^* \sim 10^{14}$).

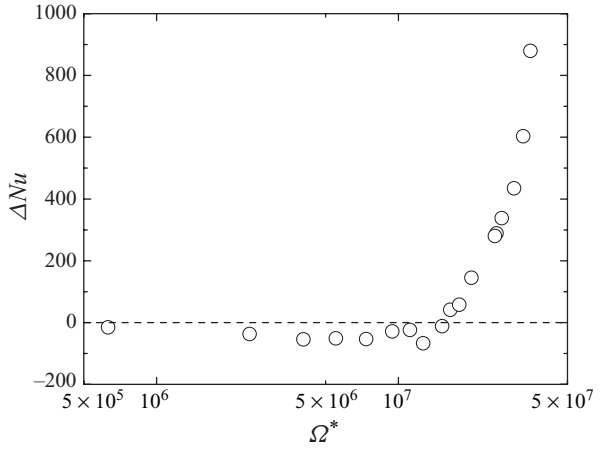

FIGURE 4. Values of ΔNu versus Ω^* for sinusoidally modulated rotation with constant $\omega = 0.168\,\mathrm{rad\,s^{-1}}$. A transition from weak suppression to significant enhancement of heat transport occurs above about $\Omega^* \sim 10^7$ ($Ta^* \sim 10^{14}$). Ra was not constant over this large range of Ω^*; the following two figures, however, consider the transition for constant Ra.

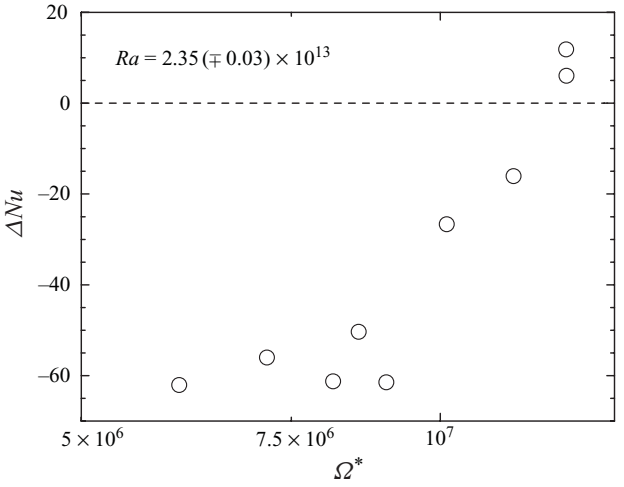

FIGURE 5. Values of ΔNu versus Ω^* for sinusoidally modulated rotation for $Ra = 2.35(\pm 0.03) \times 10^{13}$ showing the transition to enhanced heat transport for fixed Ra.

This is followed by a relatively sharp enhancement of heat transport, i.e. ΔNu becomes positive and large.

In this data set, ω was held at a fixed value of $0.168\,\mathrm{rad\,s^{-1}}$, but the large range of rotation parameters made it difficult to hold Ra fixed while also maintaining Boussinesq conditions. The special case of constant Ra (see figure 5) shows essentially the same result. It is worth noting that all enhancement occurs at high Ra, just as it does for large Ω^*. This coincidence, at least in the trend, appears to have a relatively trivial explanation: major increases in both Ω^* and Ra were obtained in the experiment by moving the operating point to regions of the pressure–temperature phase space where the kinematic viscosity is low. Indeed, plots of ΔNu against Ra

or simply against ν^{-1} are qualitatively indistinguishable. As we shall see below, Ω^* (or equivalently Ta^*) appears to be the proper 'control' parameter for the transition; nonetheless, Ra may likely play a role in the transition by determining the length and time scales in the flow.

In terms of a modulation *Reynolds number*, Re^*, defined as

$$Re^{*1/2} = H\left[\frac{2\Omega_D^*}{\nu}\right]^{1/2}, \tag{3.8}$$

the transition occurs for $Re^{*1/2}$ of a few thousand. The inverse of the quantity multiplying H in (3.8) is analogous to the viscous boundary layer in non-rotating turbulence and is the Ekman layer, δ_{Ek}^* for the modulated system defined as

$$\delta_{Ek}^* = \sqrt{\frac{\nu}{2\Omega_D^*}} = H/\Omega^{*1/2}. \tag{3.9}$$

Large Ω^* corresponds to small Ekman layer thickness and stronger pumping from the boundaries. Our definition of the Ekman layer uses molecular viscosity instead of an eddy viscosity because the heat transport dynamics is embedded primarily in the thermal boundary layer, and it appears that the relevant Ekman layer would also have to be comparable in thickness. Smaller Ekman numbers correspond to stronger pumping from the boundaries but the usual spin-up times appropriate to 'the entire container', computed for quiescent fluids, are much longer than the modulation period here. (Since the operating conditions are turbulent, it may be thought that the Ekman layer thickness would be more reasonably defined by replacing ν in (3.9) by an effective viscosity. An estimate on that basis would indeed yield thicknesses comparable to the fluid-layer thickness. One further point is that processes within the thermal boundary layer are faster than those over H by the factor $(2\,Nu)$ and would be comparable or faster than the modulation period for large Nu (or large Ra).)

As noted above, the Rayleigh number in figure 4 was not held constant; in fact, much of the variation in Ω^* was due to varying kinematic viscosity rather than the rotation amplitude Ω_D^*. In figure 5 we show a subset of the data, also illustrating the transition, for which the Rayleigh number was held constant at $Ra = 2.35(\pm 0.02)\times 10^{13}$. In figure 6 we show data obtained for Ω^* sufficiently above the transition value, for fixed heating conditions, corresponding to $Ra = 8.4(\pm 0.1)\times 10^{14}$. For these data, the increase in Ω^* was effected solely by increasing the dimensional modulation amplitude Ω_D^*. This is indeed shown in figure 6(b) while the same data are plotted against the dimensionless rotation rate in figure 6(a). In this figure, besides Ra, the modulation frequency was also fixed at $\omega = 0.168\,\mathrm{rad\,s^{-1}}$. Clearly, the factor 3 increase in ΔNu can be attributed directly to the increase in rotational speed of the container suggesting that the appropriate control parameter for the transition is, indeed, Ω^*.

As pointed out earlier, the ratio of the conduction layer to the viscous Ekman layer was considered by King *et al.* (2009) to be more relevant for convection dynamics with rotation than the Rossby number. In consideration of this idea, we have taken a further subset of data for which 'all' the modulation parameters were kept fixed ($\omega = 0.168\,\mathrm{rad\,s^{-1}}$ and $\Omega_D^* = 0.444\,\mathrm{rad\,s^{-1}}$). Varying Ra produces a change only in the thermal boundary-layer thickness while varying Ω^* produces variations only in the Ekman layer thicknesses, so the two can be varied essentially independently – except indirectly through interactions with the environment, the thermal boundary-layer thickness should have no dependence on the rotation parameters. Estimating

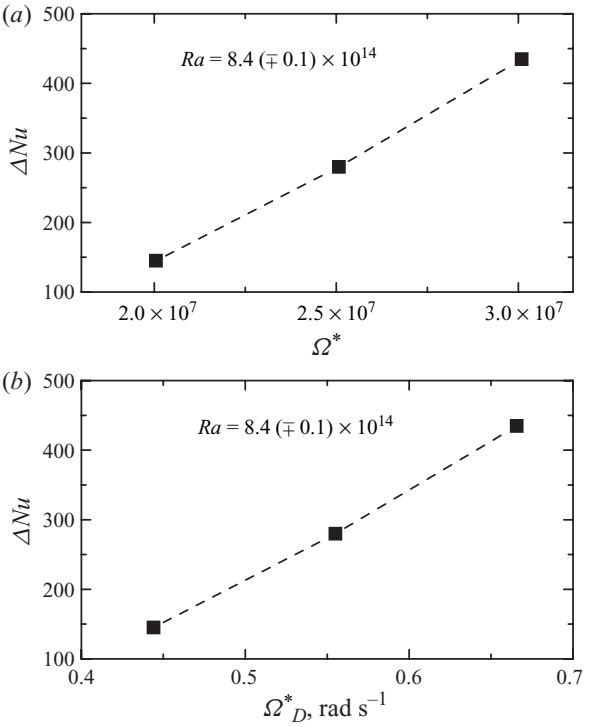

FIGURE 6. (*a*) Values of ΔNu versus Ω^* for fixed heating conditions giving $Ra = 8.4(\pm 0.1) \times 10^{14}$. For these data, $\omega = 0.168\,\mathrm{rad\,s^{-1}}$. (*b*) The same data plotted against the dimensioned amplitude Ω^*_D showing explicitly that the enhancement is directly controlled by variations in Ω^*_D and suggesting that a purely rotational control parameter is appropriate for the transition, i.e. Ω^*.

the thermal boundary-layer thickness in a standard way by

$$\delta_T = H/2Nu \tag{3.10}$$

and using the Nu–Ra relation, $Nu = 0.124Ra^{0.309}$, of Niemela *et al.* (2000) in addition to (3.9) for the Ekman layer thickness, the ratio of the two boundary-layer thicknesses is given by

$$\delta^*_{Ek}/\delta_T \cong \frac{1}{4}\frac{Ra^{0.309}}{\Omega^{*1/2}}. \tag{3.11}$$

They become equal when $Ra^{0.309}/\Omega^{*1/2} \simeq 4$. We plot δ^*_{Ek}/δ_T against $Ra^{0.309}\Omega^{*-1/2}$ in figure 7(*a*) and ΔNu against the same quantity in figure 7(*b*). The linearity of the data in figure 7(*a*) verifies (3.11). It is also the case (see figure 7*b*) that the two thicknesses are comparable when the transition to enhanced heat transport occurs, keeping in mind that the estimates are rough. Indeed, when this sharp transition to enhanced heat transport was reported first by us in 2008 (Bulletin of the American Physical Society BAPS.2008.DFD.AS.3), it was thought that such a crossing of thermal and Ekman boundary-layer thicknesses was responsible. However, this correspondence cannot be general: at a sufficiently high Ra, the thermal boundary layer always becomes embedded within the 'steady' Ekman layer in the case of fixed rotation rate, but without any enhancement of Nu. Thus, we may postulate that crossing of thicknesses is a necessary but not sufficient condition, and that the control parameter

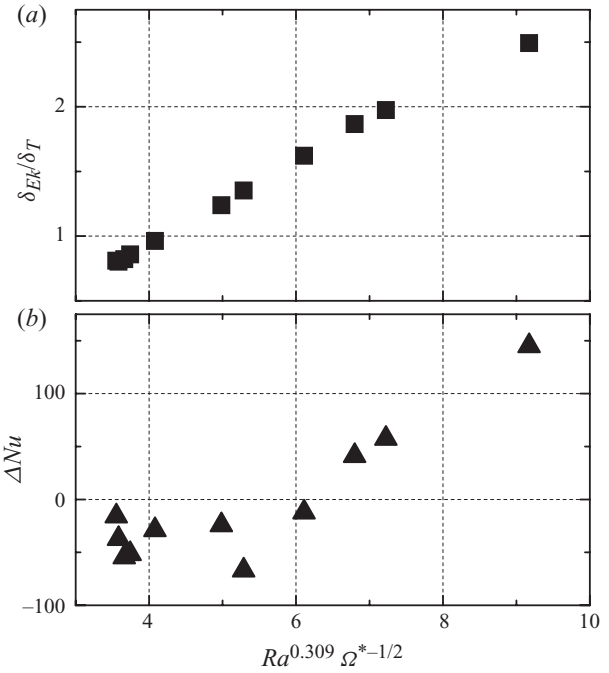

FIGURE 7. (*a*) The ratio of the modulation Ekman layer thickness to the thermal boundary-layer thickness versus $Ra^{0.309}\Omega^{*-1/2}$ (see text) for a subset of data in figure 4 for both modulation parameters are held constant: $\Omega_D^* = 0.444\,\mathrm{rad\,s^{-1}}$ and $\omega = 0.168\,\mathrm{rad\,s^{-1}}$. (*b*) ΔNu versus $Ra^{0.309}\Omega^{*-1/2}$.

for the enhancement under modulation, as indicated above, is probably a purely rotational parameter, i.e. Ω^*. It is of considerable interest to note that similarly sharp transitions under turbulent conditions have been observed recently by Stevens *et al.* (2009).

The results shown in figures 4–7 show that the crossover from a viscous-dominated system to one dominated by the Coriolis forces coincides with significantly enhanced heat transport. Clearly, there are poorly understood aspects of turbulent convection with and without rotation, and the large-scale flow (the so-called 'mean wind', see e.g. Sreenivasan, Bershadskii & Niemela 2002; Niemela & Sreenivasan 2003*b*; Ahlers *et al.* 2009) resulting from the turbulent convection itself has to be considered, even though this mean wind is rather weakly organized in small aspect ratio cells where the diameter to height ratio is 1/2 or less (see e.g. Qiu & Tong 2001).

3.3. *Time traces of the bottom plate temperature*

It is instructive to consider the bottom plate temperature T_B under rotation with and without modulation. In figure 8 we plot T_B as a function of time for $Ra = 4.3 \times 10^{15}$ when the modulated rotation (left part, with dimensional rotation rate $\Omega_D^* = 0.67\,\mathrm{rad\,s^{-1}}$, $\omega = 0.168\,\mathrm{rad\,s^{-1}}$) changes to steady rotation (right part, dimensional rotation rate $\Omega_D = 0.84\,\mathrm{rad\,s^{-1}}$). The transition from modulated to the steady state takes place through a spin-down to $\Omega^* = 0$ and a subsequent spin-up to the steady rotation after some brief waiting time. At $t = 0$, the modulation has already been operating with $\Omega^* = 3.52 \times 10^7$, above the transition value of approximately 10^7 for which an enhancement of heat transport was observed. The dashed horizontal

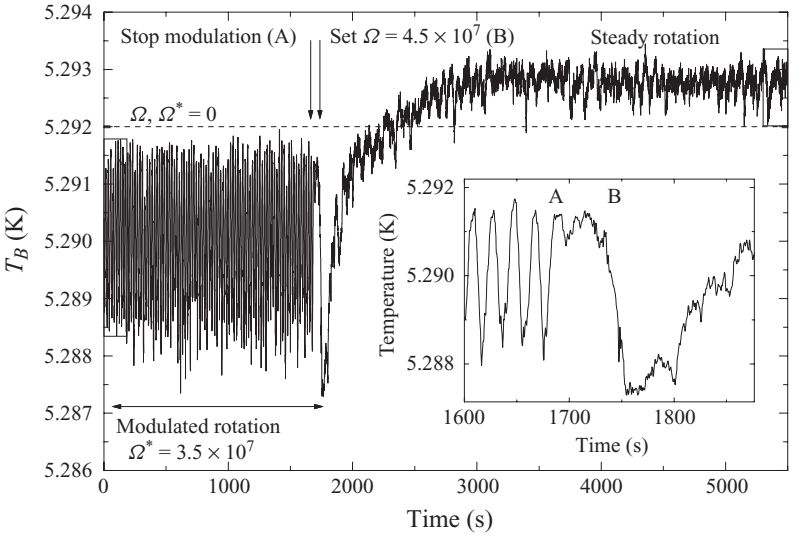

FIGURE 8. Traces of the bottom plate temperature as a function of time for $Ra = 4.3 \times 10^{15}$. The left part of the trace corresponds to modulation with $\Omega^* = 3.5 \times 10^7$ ($\Omega_D^* = 0.67\,\mathrm{rad\,s^{-1}}$), $\omega = 0.168\,\mathrm{rad\,s^{-1}}$. The modulation is stopped at the position of the left vertical arrow (labelled A), spinning down to $\Omega^* = 0$. At the position of the right vertical arrow (labelled B), there is spin-up to a steady rotation rate of $\Omega_D = 0.84\,\mathrm{rad\,s^{-1}}$ corresponding to $\Omega = 4.5 \times 10^7$. The horizontal dashed line is the mean bottom plate temperature for no rotation. For the modulation, $\delta_{Ek}^*/\delta_T = 3.35$. The inset shows an expanded view of the transition region from modulation to impulsive spin-up via the no-rotation state. The large and periodic thermal signals in the plate at twice the period of modulation, as well as the large temperature spike immediately following the impulsive spin-up from rest, are presumably due to Ekman pumping from the boundary.

line shows the mean value of the bottom plate temperature for the same heating conditions with no rotation. Since the top plate temperature was held fixed, it is easy to see the enhancement effect on heat transport from T_B, which is in the form of large 'cold' spikes in the temperature, providing direct evidence of a strong pumping action. The modulation is then stopped at the left vertical arrow (labelled 'A'), with the apparatus spinning down momentarily to $\Omega^* = 0$. After a brief interval, the apparatus was spun up to a steady rotation rate $\Omega_D = 0.84\,\mathrm{rad\,s^{-1}}$ at the right vertical arrow ('B') corresponding to $\Omega = 4.5 \times 10^7$. Even though the Ekman boundary layer for this steady rotation is considerably larger than the thermal boundary layer, there is no corresponding enhancement of heat transfer.

An expanded view of the transition is shown in the inset. Here it is clear that the modulation produces large cold spikes in the bottom plate indicative of intense impulsive heat transport events that produce large thermal 'holes' in the plate temperature at the frequency of 2ω. The spin-up of the apparatus from rest to steady rotation also produces a large cold spike in the temperature trace as shown, after which the system relaxes to steady state at $\Omega = 4.5 \times 10^7$ ($Ta = 2 \times 10^{15}$) at which the bottom plate temperature is now warmer than that for the modulated case as well as the non-rotating case with depressed Nu.

Finally, we illustrate in figure 9 the bottom plate signals for modulated convection when Ω^* is well above (a) and just below (b) the transition value of $\Omega^* \approx 10^7$. Figure 9(a) corresponds to $\Omega^* = 3.52 \times 10^7$ and $\delta_{Ek}^*/\delta_T = 3.35$, same as for the leftmost

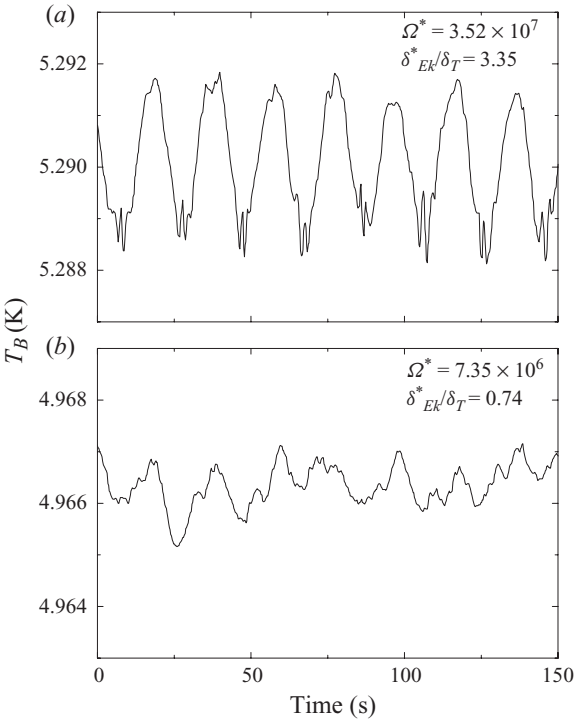

FIGURE 9. Time traces of the bottom plate temperature for two cases of modulated rotation. (*a*) $\Omega^* = 3.52 \times 10^7$, $\delta^*_{Ek}/\delta_T = 3.35$. (*b*) $\Omega^* = 7.35 \times 10^6$, $\delta^*_{Ek}/\delta_T = 0.74$. The period of modulation for both cases is the same: $\omega = 0.168\,\mathrm{rad\,s^{-1}}$. The temperature range on the ordinate is also the same. Large periodic cold spikes appear only for the conditions in (*a*) ($\Omega^* > 10^7$, $\delta^*_{Ek}/\delta_T > 1$).

part of figure 8 and shows large cold spikes indicative of strong pumping during the modulation cycle for this Ω^*. Figure 9(*b*) corresponds to conditions just below transition, $\Omega^* = 7.35 \times 10^6$ and $\delta^*_{Ek}/\delta_T = 0.74$. For both cases, $\omega = 0.168\,\mathrm{rad\,s^{-1}}$ and the modulation amplitudes are quite similar ($\Omega^*_D = 0.67, 0.59\,\mathrm{rad\,s^{-1}}$, respectively). The pronounced difference in the time traces shows clearly that the modulation has no significant effect on the wall temperature for conditions of figure 9(*b*).

4. Concluding remarks

We have investigated both steady and time-varying rotating turbulent convection for *Ra* up to 4.3×10^{15} and *Ta* up to 3×10^{15} in the steady case; the Rossby number varied from 0.4 to 1.6. Unlike in previous experimental investigations at lower *Ra* and *Ta*, but similar *Ro* and *Pr*, steady rotation results only in a mild suppression of heat transport. This suppression follows weak power laws in both *Ta* and (inverse) *Ro*, and was shown to be so for moderate $Pr = 5.9$ similar to that of water. The present results are consistent with those of Zhong *et al.*, which show that the enhancement of heat transport decreases as *Ra* is increased (their observations extended up to 1.8×10^{10}). In the recent work by King *et al.* (2009), the influence of *Ro* is considered secondary in importance to the ratio of boundary-layer thicknesses to the Ekman layer thickness. In these measurements, this ratio is of the order unity.

The sinusoidal modulation of the rotation rate also suppresses heat transport for time-dependent rotation rates $\Omega^* < 10^7$ ($Ta^* < 10^{14}$); clearly, for these conditions,

Ekman pumping does not operate efficiently. Above this transitional value, however, we observe a sharp enhancement of heat transport, coinciding with the occurrence of large cold spikes in the bottom plate temperature at the frequency of the rectified modulation. To our knowledge, this transition has not been reported previously. When Ra is held constant (including constant ν), it is clear that the enhancement in heat transport with increasing Ω^* is directly attributable to increases in the rotation rate. From a subset of data for which all the modulation parameters were held constant, we found that the transition to enhanced heat transport occurred roughly when the Ekman layer nominally exceeded the thermal boundary layer in thickness. However, this condition does not yield the same result in steady rotation.

Neither the Ekman layer thickness of (3.9) nor the thermal boundary-layer thickness has been directly measured, which makes conclusions based on their estimated thicknesses less than firm. The value of such estimates has to be tempered by the time-varying emission of plumes and the existence of strong fluctuations. While it appears clear that an effective (and much larger) turbulent viscosity would lead to an Ekman layer thickness comparable to the cell height (thus making it less relevant to the problem of heat transport), it is conceivable that an intermediate height would be relevant to the heat transport problem (see e.g. Niemela & Sreenivasan 2008).

Finally, we remark that rotating convection at very high Rayleigh numbers has not received the same attention as the case of non-rotating systems. It is of obvious importance to many geophysics and astrophysics problems, and it is hoped that future studies will be able to address this issue. It is also important to study this problem through direct numerical simulations, which will enable proper estimates of various flow parameters to be made in greater detail.

We thank the Elettra Synchrotron Light Laboratory, Trieste, for providing laboratory space for these experiments, Snaidero Corporation for providing, as a gift, a platform for the rotating electronics and Margarita Kuqali of the Polytechnic University of Tirana for some assistance with experiments.

REFERENCES

Ahlers, G. 2001 Effect of sidewall conductance on heat-transport measurements for turbulent Rayleigh–Bénard convection. *Phys. Rev.* E **63**, 015303.

Ahlers, G., Grossmann, S. & Lohse, D. 2009 Heat transfer and large scale dynamics in turbulent Rayleigh–Bénard convection. *Rev. Mod. Phys.* **81**, 503–537.

Chandrasekhar, S. 1961 *Hydrodynamic and Hydromagnetic Stability*. Oxford University Press.

Julien, K., Legg, S., McWilliams, J. & Werne, J. 1996 Hard turbulence in rotating Rayleigh–Bénard convection *Phys. Rev.* E **53**, R5557–R5560.

King, E. M., Stellmach, S., Noir, J., Hansen, U. & Aurnou, J. M. 2009 Boundary layer control of rotating convection systems. *Nature* **457**, 301–304.

Kunnen, R. P. J., Clercx, H. J. H. & Geurts, B. J. 2006 Heat flux intensification by vortical flow localization in rotating convection. *Phys. Rev.* E **74**, 056306.

Kunnen, R. P. J., Clercx, H. J. H. & Geurts, B. J. 2008 Breakdown of large-scale circulation in turbulent rotating convection. *Europhys. Lett.* **84**, 24001.

Liu, Y. & Ecke, R. E. 1997 Heat transport scaling in turbulent Rayleigh–Bénard convection: Effects of rotation and Prandtl number *Phys. Rev. Lett.* **79**, 2257–2260.

Niemela, J. J., Smith, M. R. & Donnelly, R. J. 1991 Convective instability with time-varying rotation. *Phys. Rev.* A **44**, 8406–8409.

Niemela, J. J., Skrbek, L., Sreenivasan, K. R. & Donnelly, R. J. 2000 Turbulent convection at very high Rayleigh numbers. *Nature* **404**, 837–840.

Niemela, J. J. & Sreenivasan, K. R. 2003*a* Confined turbulent convection *J. Fluid Mech.* **481**, 355–384.

Niemela, J. J. & Sreenivasan, K. R. 2003*b* Rayleigh number evolution of large scale coherent motion in turbulent convection. *Europhys. Lett.* **62**, 829–833.

Niemela, J. J. & Sreenivasan, K. R. 2006 The use of cryogenic helium for classical turbulence: promises and hurdles. *J. Low Temp. Phys.* **143**, 163–212.

Niemela, J. J. & Sreenivasan, K. R. 2008 Formation of the 'Superconducting' core in turbulent thermal convection. *Phys. Rev. Lett.* **100**, art. no. 184502.

Oresta, P., Stringano, G. & Verzicco, R. 2007 Transitional regimes and rotation effects in Rayleigh–Bénard convection in a slender cylindrical cell. *Eur. J. Mech.* B/*Fluids* **26**, 1–14.

Qiu, X.-L. & Tong, P. 2001 Large-scale velocity structures in turbulent thermal convection. *Phys. Rev.* E **64**, 036304.

Rossby, H. T. 1969 A study of Bénard convection with and without rotation. *J. Fluid Mech.* **36**, 309–335.

Sreenivasan, K. R., Bershadskii, A. & Niemela, J. J. 2002 Mean wind and its reversal in thermal convection. *Phys. Rev.* E **65**, 056306.

Stevens, R. J. A. M., Zhong, J.-Q., Clercx, H. J. H., Ahlers, G. & Lohse, D. 2009 Transitions between turbulent states in rotating Rayleigh–Bénard convection. *Phys. Rev. Lett.* **103**, 024503.

Thompson, K. L., Bajaj, K. M. S. & Ahlers, G. 2002 Traveling concentric-roll patterns in Rayleigh–Benard convection with modulated rotation. *Phys. Rev.* E **65**, 046218.

Tritton, D. J. 1988 *Physical Fluid Dynamics.* Clarendon.

Verzicco, R. 2002 Side wall finite conductivity effects in confined turbulent thermal convection. *J. Fluid Mech.* **473**, 201–210.

Zhong, F., Ecke, R. E., & Steinberg, V. 1993 Rotating Rayleigh–Bénard convection: asymmetric modes and vortex states. *J. Fluid Mech.* **249**, 135–159.

Zhong, J.-Q, Stevens, R. J. A. M., Clercx, H. J. H., Verzicco, R., Lohse, D. & Ahlers, G. 2009 Prandtl-, Rayleigh-, and Rossby-number dependence of heat transport in turbulent rotating convection. *Phys. Rev. Lett.* **102**, 044502.